



# Random error analysis of profile measurement of large aspheric optical surface using scanning deflectometry with rotation stage

Muzheng Xiao\*, Tomohiko Takamura, Satoru Takahashi, Kiyoshi Takamasu

Department of Precision Engineering, School of Engineering, The University of Tokyo, Japan

## ARTICLE INFO

### Article history:

Received 8 August 2012  
 Received in revised form  
 26 December 2012  
 Accepted 8 January 2013  
 Available online 20 January 2013

### Keywords:

Profile measurement  
 Aspheric optical surface  
 Scanning deflectometry  
 Random error analysis

## ABSTRACT

Scanning deflectometry method has been successfully employed for the measurements of large flat surfaces with sub-nanometer uncertainty. In this paper, we propose an alternative scanning deflectometry method for measuring large aspheric optical surfaces, wherein a rotation stage is incorporated to increase the measurement range of the high-accuracy autocollimators used to measure small angles. Further, the pitching error of the linear stage is compensated with offline measurement data. In this study, we conducted random error analysis to estimate the measurement repeatability. Our results show that for the measurements of large aspheric surfaces with large slope changes, 10-nm repeatability is achievable under the suitable conditions. To verify the random error analysis results, we also constructed an experimental setup for test the measurement repeatability. The repeatability distribution of the experimental results was in good agreement with the error analysis distribution. We have thus demonstrated the applicability of the random error analysis in the measurement of large aspheric surfaces with high accuracies.

© 2013 Elsevier Inc. All rights reserved.

## 1. Introduction

Large aspheric optical surfaces are extensively used in high-tech industries such as facilities for constructing large telescopes and for obtaining synchrotron radiation. However, the accuracies of these surfaces are typically less than hundreds of nanometers [1]. Hence, profile measurement of optical surfaces with high accuracies must be conducted in order to ensure that their uncertainty is less than tens of nanometers.

Interferometers employing holograms or null methods are also used for measuring aspheric optical surfaces that exhibit slight departures from a perfect sphere [2,3]. Stitching interferometers have also been developed to measure aspheric surfaces with departures less than 1000 waves from perfect spherical surfaces.

As an absolute measurement method to measure optical flat surfaces, scanning deflectometry using an autocollimator has been proposed previously [4,5]. The experimental results show that sub-nanometer uncertainty is acquired with both repeatability and reproducibility [4]. However, because high-accuracy autocollimators have limited measurement ranges, it cannot be used for the measurement of surfaces with large slope changes. To increase the measurement range of high-accuracy autocollimators, a scanning

deflectometry method with rotatable devices has been proposed [6]. In this method, double reflection is applied to eliminate the pitching errors of the linear stage; the experiment results demonstrate that the measurement range was increased. However, the distribution of measurement repeatability did not coincide with the error analysis results calculated using the traditional formula.

In this paper, we have proposed an alternative scanning deflectometry method for the measurement of large aspheric optical surfaces, which incorporates a rotation stage. In this method, random error analysis is performed with both the error propagation method and Monte Carlo method. Further, we have constructed an experiment setup for verifying the random error analysis and we conducted repeated measurement experiments. The distribution of the measurement repeatability has very good agreement with the random error analysis results.

## 2. Principle

### 2.1. Principle of scanning deflectometry

The scanning deflectometry method is extremely popular for the measurements of slightly sloped optical surfaces; here, the changes in the slope of the optical surface (normal) are scanned by an angle sensor. The surface profile is indirectly obtained by integrating the angle data. To eliminate the effects of the pitching error of the linear scanning stage, a pentaprism is fixed on the linear stage, as shown in Fig. 1. The light beam from the autocollimator is then reflected

\* Corresponding author.

E-mail addresses: [xiaomuzheng@nanolab.t.u-tokyo.ac.jp](mailto:xiaomuzheng@nanolab.t.u-tokyo.ac.jp), [muzheng.xiao@bit.edu.cn](mailto:muzheng.xiao@bit.edu.cn), [xiao-mu-zheng@hotmail.com](mailto:xiao-mu-zheng@hotmail.com) (M. Xiao).

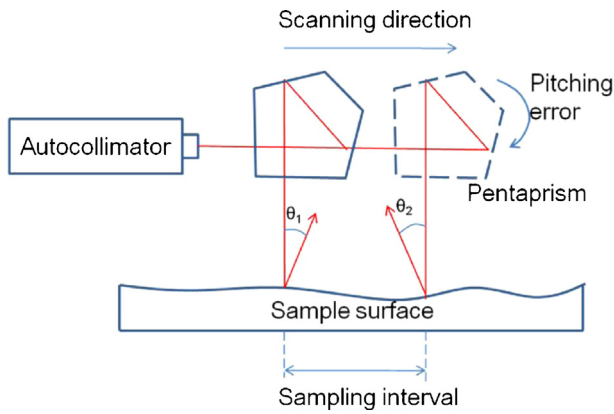


Fig. 1. Principle of scanning deflectometry with autocollimator and pentaprism.

twice by the pentaprism, thereby eliminating the pitching error of the linear stage.

2.2. Scanning deflectometry method with rotation stage

Because of the limited measurement range of high-accuracy autocollimators, the scanning deflectometry method cannot be employed for measuring surfaces with large slope changes.

Hence, in our study, we employed a rotation stage in order to increase the measurement range of the autocollimator. As shown in Fig. 2, we first fixed a rotation stage between the linear stage and autocollimator and then turned it at a certain angle when the angle detected by the autocollimator reached a limit; the autocollimator then displayed the angle. In this manner, the rotation stage increases the measurement range.

Similar to the traditional scanning deflectometry method, pitching error of linear stage (Fig. 2) significantly affects the measured angle. As shown in Fig. 3, two compensation methods are proposed to eliminate the effects of the pitching error offline and online compensation methods.

In the case of the offline compensation method, the compensation accuracy depends on the combined error from error of autocollimator and the repeatability of the pitching angle of the linear stage, whereas, for online compensation, the accuracy only depends on the autocollimator. As a result, online compensation has higher accuracy than offline compensation. Nevertheless, in this paper, we have used the offline compensation method for the pitching error because it is easier to construct the experimental setup. The pitching error of the linear stage is measured in advance and the data is used to compensate the angle change data of the sample surface.

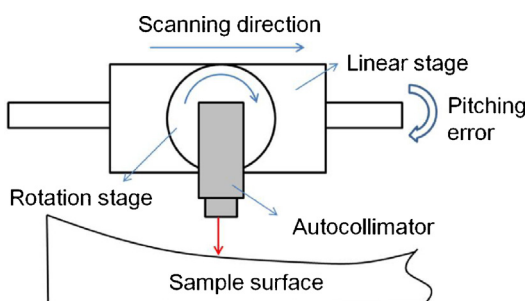


Fig. 2. Principle of scanning deflectometry method with rotation stage.

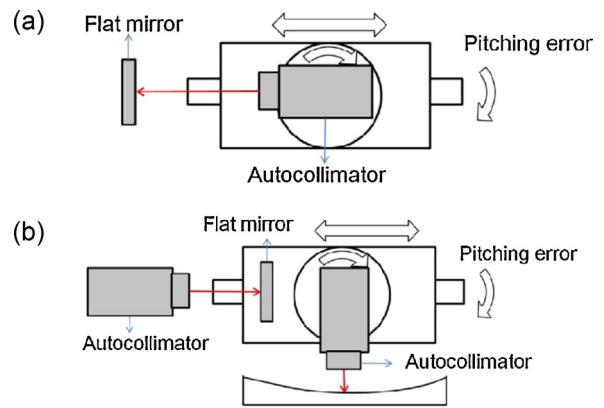


Fig. 3. (a) Online and (b) offline compensation methods, for pitching error.

2.3. Data processing

In the proposed method, the profiles of the optical surfaces are not measured directly. We must first calculate the raw angle data in order to obtain the final profile data by data processing. There are primarily two steps – angle connection and profile integration.

2.3.1. Angle connection

Because of the rotation of the autocollimator, the obtained angle data  $a_i$  is interrupted. The connected angle data  $A_{ij}$  is equal to the sum of the raw angle data  $a_i$ , rotated angle  $\alpha_j$ , and the pitching error of the linear stage,  $Ep_i$ , as shown in Eq. (1).

$$A_{ij} = a_i + \sum_1^j \alpha_j + Ep_i \tag{1}$$

where  $i$  is the scanned time for the linear stage, and  $j$  is the rotation time for the rotation stage.

For precise measurements, the rotated angle must be known with high accuracy. Hence, instead of using the high-accuracy rotation stage, we have proposed a method to calculate the rotation angle indirectly with high accuracy. As shown in Fig. 4, the following relation exists between  $\alpha$  and  $\beta$ :

$$\alpha = \frac{R}{R - D} \beta \tag{2}$$

Here  $R$  is the curvature radius of the surface in the rotated part of the sample surface, and  $D$  is the distance between the rotation center and sample surface.

Because the rotation causes very small displacement changes on the surface, the curvature radius  $R$  can be estimated by the slope

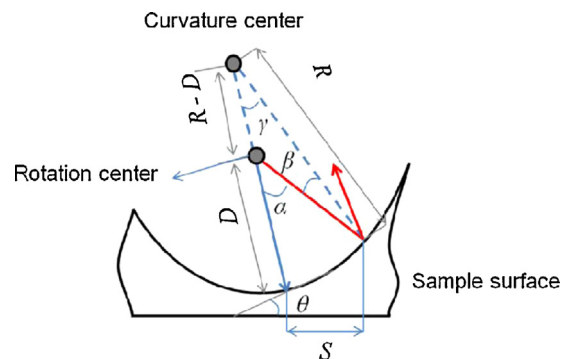


Fig. 4. Relationship between rotated angle  $\alpha$  for rotation stage and angle change  $\beta$  detected by autocollimator.

$k$  of the least square line for the angle data before rotation. The distance  $D$  is adjusted and measured before the scanning.

As the autocollimator rotates, the measured position  $X_{ij}$  on the sample surface is changed by  $S_j$  accordingly as shown in Fig. 4. The geographic relation  $S_j$  can be calculated as follows:

$$S_j = 2D \sin\left(\frac{\alpha_j}{2}\right) \cos(\theta_j) \quad (3)$$

where  $\theta_j$  is the slope on the rotation part.

The measurement position  $X_{ij}$  on the sample surface is able to be determined by two parameters: position change  $x_i$  of linear sampling and position change  $S_j$  by rotation. The position change  $x_i$  and the sampling interval  $h$  have a relation as shown in Eq. (4). The position  $X_{ij}$  can then be calculated as Eq. (5).

$$x_i = h \cos(\theta_i)^2 \quad (4)$$

$$\begin{aligned} X_{ij} &= \sum x_i + \sum S_j \\ &= h \sum \cos(\theta_i)^2 + 2D \sum \sin\left(\frac{\alpha_j}{2}\right) \cos(\theta_j) \end{aligned} \quad (5)$$

### 2.3.2. Profile integration

By using the connected angle data  $A_{ij}$  and the corresponding position on the surface,  $X_{ij}$ , the surface profile  $F_{ij}$  can be calculated using the numerical integration method based on the trapezoidal rule, as shown in Eq. (6).

$$\begin{aligned} F_0 &= 0 \\ A_0 &= 0 \\ F'_{ij} &= \tan(A_{ij}) \\ F_{ij} &= F_{ij-1} + (X_{ij} - X_{ij-1}) \left( \frac{F'_{ij-1} + F'_{ij}}{2} \right) \end{aligned} \quad (6)$$

In the integration process, the profile data of the first measured point is set as the origin. Subsequently, the slope of the least square line is defined as the origin of slope. Hence, the profile is subtracted by its least square line in order to obtain the slope origin.

## 3. Random error analysis

Because of the introduction of the rotation stage, the proposed method has a different structure from the traditional methods. Hence, it is necessary to perform error analyses to investigate the types of conditions required for measurements with the expected uncertainty. In this paper, only the random error is analyzed, and the systematic error is not considered. Hence, the following analysis results show the relationship between the error factors and measurement repeatability but not the measurement uncertainty.

Many error factors exist in the measurement system, but only a few affect the measurement results significantly. We have compared the effects of these error factors and determined the key error factors. Subsequently, we have elucidated the manner in which the error is propagated from the key error factors to the random errors of the final profile.

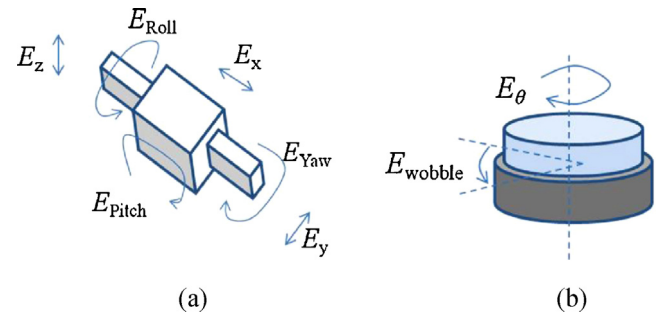


Fig. 5. (a) Motion errors of linear stage. (b) Motion errors of rotation stage.

### 3.1. Key random error factors

There are two types of random error factors: random autocollimator errors and random errors of the moving parts. Note that the random error  $E_{act}$  of the autocollimator is considered as one of the key random error factors since it directly affects the measured angle.

As shown in Fig. 2, the system has two moving parts: a linear stage and a rotation stage. The linear stage has six motion errors as shown in Fig. 5(a): positioning error  $E_x$ , straightness error on the  $Y$  direction,  $E_y$ , straightness error on the  $Z$  direction,  $E_z$ , pitching error  $E_{pitch}$ , yawing error  $E_{yaw}$ , and rolling error  $E_{roll}$ . Furthermore, the rotation stage has two error factors: the rotation positioning error  $E_\theta$  and wobble angle error  $E_w$ , as shown in Fig. 5(b).

Two motion error factors – the straightness error  $E_z$  of the linear stage in the  $Z$  direction and yawing error  $E_{yaw}$  of the linear stage do not affect the angle measurements at all. Moreover, since the pitching error of the linear stage is compensated by the offline measured data, the effects of  $E_{pitch}$  can be converted to the repeatability of the pitching error  $E_{rep}$ . Because the rotated angle of the rotation stage is measured indirectly by the autocollimator (Section 2), the effects of the positioning error  $E_\theta$  are also converted to the autocollimator error.

The relation between the motion errors and the angle errors caused by them is easy to calculate from the geometric relation. To compare the angle errors caused by different error factors, the motion error factors are considered with a similar scale, as listed in Table 1.

In this table,  $R$  is the curvature radius of the center of the parabola surface being measured;  $D$ , the distance between the center of rotation and sample surface;  $h$ , the sampling interval of the linear stage; and  $\beta$ , the change in the angle between the rotation and post-rotation detected by the autocollimator.

From the comparison results, the angle errors caused by  $E_y$ ,  $E_{roll}$ , and  $E_w$  can be neglected when compared to the effects of  $E_x$  and  $E_{rep}$ . Hence, in addition to the autocollimator error  $E_{act}$ , there are two key motion error factors: the positioning error  $E_x$  of the linear stage and the repeatability  $E_{rep}$  of the pitching error of the linear stage.

Table 1  
Parameters used in error calculations and the angle error caused by motion error factors.

Parameters used in calculations	$R$ (mm)	$D$ (mm)	$h$ (mm)	$\beta$ ( $\mu$ rad)	
Value	2000	50	1	500	
Error factors	$E_x$ ( $\mu$ m)	$E_y$ ( $\mu$ m)	$E_{rep}$ ( $\mu$ rad)	$E_{roll}$ ( $\mu$ rad)	$E_w$ ( $\mu$ rad)
Value	10	10	1.5	20	20
Angle error ( $\mu$ rad)	5	1.3e–12	1.5	3e–14	1e–27

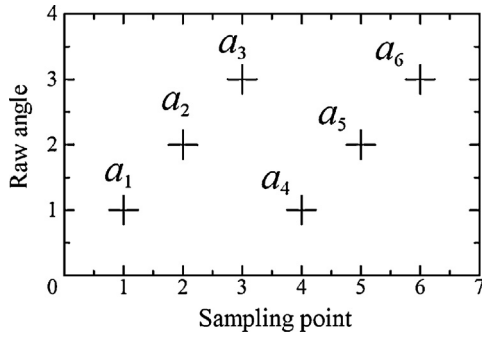


Fig. 6. Example with 6 raw angle data.

### 3.2. Error propagation

By calculating the angle error caused by the error factors, the key error factors are found to be  $E_{act}$ ,  $E_x$ , and  $E_{rep}$ . Hence, the angle error should be combined to obtain the angle random error.

The random error of the autocollimator and the repeatability of the pitching angle of the linear stage directly affect the measured raw angle. The angle measurement error caused by the positioning error is equal to  $E_x$  divided by the curvature radius  $R$  of the sample surface. As a result, the angle random errors caused by the three key error factors are combined to determine the random error  $E_a$  of the raw angle data as follows:

$$E_a = \sqrt{E_{act}^2 + \left(\frac{E_x}{R}\right)^2 + E_{rep}^2} \quad (7)$$

As introduced in Section 2, not all the calculation functions from raw angle data to final profile data are linear calculations. Nevertheless, for easier calculations, we have made several approximations in the following error propagation process. The validity of these approximations was verified by comparing the error propagation calculation results with the Monte Carlo simulation results.

Based on the linear uncertainty propagation principle, if the relation between a vector  $Q$  with  $m$  components and vector  $P$  with  $n$  components is as shown in Eq. (8), the random error variance–covariance matrix  $V_Q$  of  $Q$  and random error variance–covariance matrix  $I_p$  of  $P$  has the relation given in Eq. (9) [7].

$$Q = CP \quad (8)$$

$$V_Q = CI_pC^T \quad (9)$$

where  $C$  is the Jacobian matrix of  $Q$ .

We have given a simple example to understand the propagation process easily. Let us assume that the linear stage scans four times with a scanning interval  $h$ , and the rotation stage is rotated once after the second linear scanning. As a result, the autocollimator obtains 6 angle data  $a_i$ , as shown in Fig. 6. To simplify the calculations, the pitching angle  $Ep_i$  has already been added to the raw angle data  $a_i$ .

The rotation stage turns an angle  $\alpha$  after the autocollimator obtains the angle  $a_3$  and  $a_4$  is the angle measured after the rotation. The difference between  $a_3$  and  $a_4$  is  $\beta$  in Eq. (2).

The first step of the data processing is to calculate the rotated angle  $\alpha$  with the raw angle  $a_i$  using Eq. (2). The curvature radius  $R$  is calculated using the slope  $k$  of the least square line of the raw

angle data before rotation, i.e.,  $a_1$ ,  $a_2$ , and  $a_3$ . Eq. (2) is transformed into Eq. (10) in this example.

$$R = \frac{1}{k}; \beta = a_3 - a_4; \quad (10)$$

$$\alpha = \frac{1}{1 - (a_3 - a_1/2h)D}(a_3 - a_4)$$

The vector  $Q_1$  ( $a_1, a_2, \dots, a_6, \alpha$ ) and raw angle vector  $R_A$  ( $a_1, a_2, \dots, a_6$ ) have the following relationship:

$$Q_1 = C_1 R_A \quad (11)$$

where the Jacobian matrix  $C_1$  is calculated as Eq. (12).

$$C_1 = \begin{pmatrix} 1 & 0 & 0 & 0 & 0 & 0 \\ 0 & 1 & 0 & 0 & 0 & 0 \\ 0 & 0 & 1 & 0 & 0 & 0 \\ 0 & 0 & 0 & 1 & 0 & 0 \\ 0 & 0 & 0 & 0 & 1 & 0 \\ 0 & 0 & 0 & 0 & 0 & 1 \\ \frac{\partial \alpha}{\partial a_1} & 0 & \frac{\partial \alpha}{\partial a_3} & \frac{\partial \alpha}{\partial a_4} & 0 & 0 \end{pmatrix} \quad (12)$$

We assume that the raw angles have the same random errors with the standard deviation of one, and moreover, that the raw angle data is independent of each other; the variance–covariance matrix  $I$  of the raw angle error is the identity matrix of size 6. Subsequently, the variance–covariance matrix  $V_1$  of  $Q_1$  is calculated using Eq. (13).

$$V_1 = C_1 I C_1^T \quad (13)$$

The connected angle  $A$  is calculated with the raw angle and rotation angle vector  $R_A$  using

$$A_{ij} = C_2 R_A \quad (14)$$

The Jacobian matrix  $C_2$  of the connected angle  $A$  is

$$C_2 = \begin{pmatrix} 1 & 0 & 0 & 0 & 0 & 0 \\ 0 & 1 & 0 & 0 & 0 & 0 \\ 0 & 0 & 1 & 0 & 0 & 0 \\ 0 & 0 & 0 & 1 & 0 & 0 \\ 0 & 0 & 0 & 0 & 1 & 0 \\ 0 & 0 & 0 & 0 & 0 & 1 \end{pmatrix} \quad (15)$$

Finally, the variance–covariance matrix  $V_2$  of  $A$  is calculated as follows:

$$V_2 = C_2 V_1 C_2^T \quad (16)$$

The calculation from the connected angle  $A$  to the profile data  $F$  is introduced in Eq. (5). To simplify the calculations, in this error propagation, we make the approximation that the angle tangent equals the angle. The resulting profile vector  $F$  calculated from connected angle vector  $A$  and position vector  $X$  is given by

$$F = C_3 A \quad (17)$$

The Jacobian matrix  $C_3$  of the profile data  $F$  is

$$C_3 = \begin{pmatrix} 0 & 0 & 0 & 0 & 0 & 0 \\ 0 & h & 0 & 0 & 0 & 0 \\ 0 & h & h & 0 & 0 & 0 \\ 0 & h & h & s & 0 & 0 \\ 0 & h & h & s & h & 0 \\ 0 & h & h & s & h & h \end{pmatrix} \quad (18)$$

Here  $s$  is the change in the distance by the rotation calculated using Eq. (3) and  $h$  is the scanning interval of the linear stage.

**Table 2**  
Parameters used in angle error propagation.

	Parameters				
	$L$ (mm)	$R$ (mm)	$h$ (mm)	$A_{max}$ ( $\mu\text{rad}$ )	$D$ (mm)
Value	300	2000	1	10,000	20

	Parameters		
	$E_{act}$ ( $\mu\text{rad}$ )	$E_x$ ( $\mu\text{m}$ )	$E_{rep}$ ( $\mu\text{rad}$ )
Value	0.1	0.1	0.1

The variance–covariance matrix  $V_3$  of the profile data  $F$  is subsequently calculated as follows:

$$V_3 = C_3 V_2 C_3^T \tag{19}$$

Since the data processing was introduced in Section 2, we make the least square line as the slope standard of the profile; hence, the profile vector  $F$  is subtracted and we obtain the final profile vector  $G$ . Finally, the propagation calculation from the raw angle data to the final profile data is performed.

### 3.3. Error propagation example

In order to clearly observe and understand the propagation result, we will now describe an analysis example for measuring the parabola surface. The measurement conditions and the parameters of the sample surface are listed in Table 2.

In Table 2,  $L$  is the length of the sample surface;  $h$ , the sampling interval of the linear stage;  $R$ , the center curvature radius of the parabola surface;  $D$ , the distance between the rotation center of the rotation stage and sample surface;  $E_{act}$ , the autocollimator error;  $E_x$ , the positioning error of the transmission stage; and  $E_{rep}$ , the repeatability of the pitching angle of the linear stage.

The random error distribution of the connected angle is shown in Fig. 7.

In this simulation, the measurement range is 10,000  $\mu\text{rad}$  and is smaller than the angle range of the sample surface, 148,900  $\mu\text{rad}$ ; hence, the rotation stage rotated 14 times. From Fig. 7, when the rotation stage rotated, the connected angle error increased significantly; this implies that the connected angle has a larger error when the rotation time is greater.

Fig. 8 shows the random error distribution of the final profile.

The random error is large at the beginning, end, and middle parts of the surface. The smallest error occurs on the two points wherein the profile intersected with the least square line. The mean of the random profile error is 12 nm. This implies that under the given conditions, it is feasible to achieve high measurement repeatability of around ten nanometers by using the proposed method.

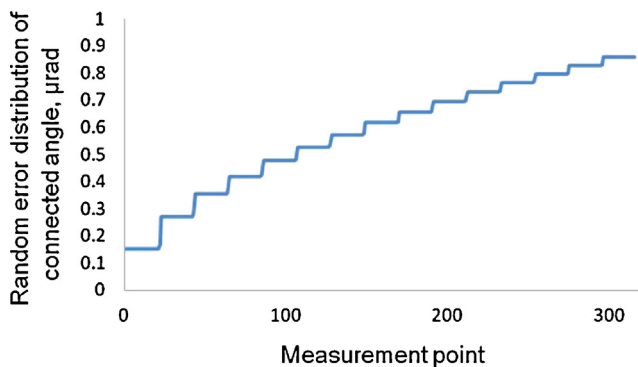


Fig. 7. Random error distribution of connected angle.

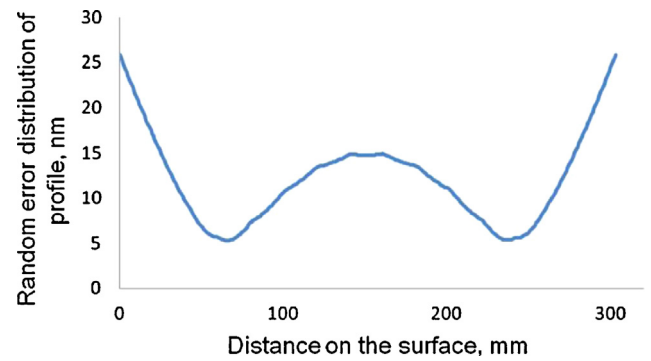


Fig. 8. Random error distribution of final profile  $g_x$ .

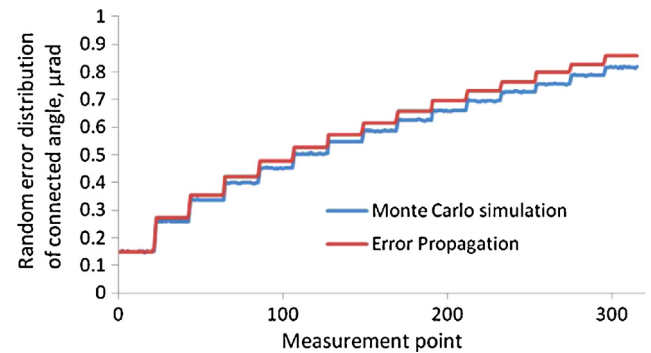


Fig. 9. Error distribution of connected angle, calculated from Monte Carlo simulations.

### 3.4. Monte Carlo calculations

Since the linear propagation process has many approximations, it is necessary to verify the extent of the difference from the calculations with the nonlinear model without approximation. We performed Monte Carlo simulations with 10,000 calculations in order to verify the validity of the random error propagation calculations. The parameters in the Monte Carlo simulation are identical to those given in Table 1. The connected angle error distribution is compared with the error propagation results (Fig. 9), and the final profile error distribution is compared with the error propagation results (Fig. 10).

From Figs. 9 and 10, the Monte Carlo simulation results are similar to the random error distributions calculated using the error propagation with approximation; the error propagation result is larger but the difference is only around 6 percent, which is

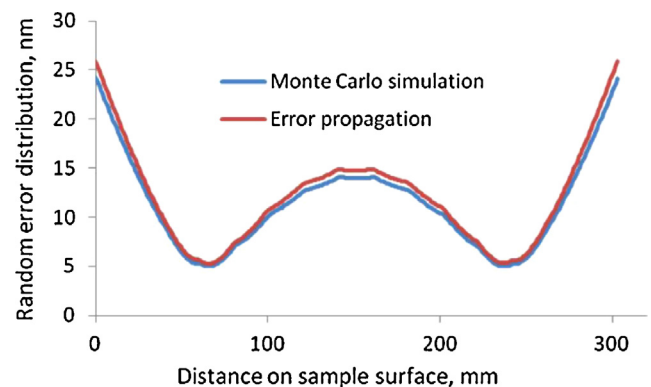


Fig. 10. Error distribution of final profile, calculated from Monte Carlo simulations.

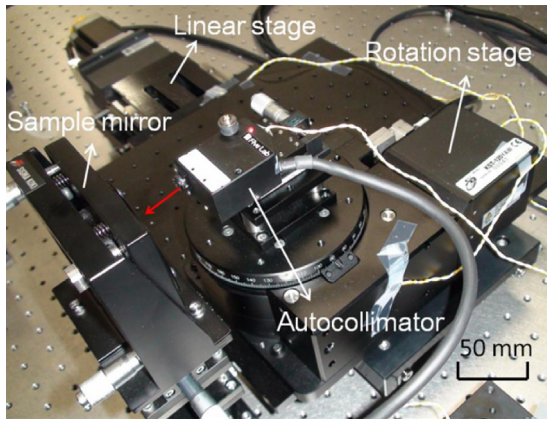


Fig. 11. Experiment setup with proposed method.

sufficiently small. In this manner, the error propagation process has been proved to have high validity.

The simulation results also show that under the given measurement conditions, measurement repeatability of around 10 nm can be achieved with the proposed method.

#### 4. Experiment

To verify the basic principles of the proposed method and the validity of the error analysis results, we constructed the experimental setup shown in Fig. 11.

A linear stage with a moving range of 200 mm and positional repeatability of  $2 \mu\text{m}$  was used for linear scanning. A rotation stage was fixed on the linear stage, and an autocollimator was placed on top of the stage. The measurement range of the autocollimator was  $\pm 100$  arc-second, i.e., around  $\pm 485 \mu\text{rad}$ .

The stability of the autocollimator was measured in advance, as shown in Fig. 12. The standard deviation of the autocollimator stability was 0.06 arc-second, i.e.,  $0.3 \mu\text{rad}$ , and this was considered to be the random error of the autocollimator.

The pitching error of the linear stage was also tested with repeated measurements (10 times), and the results are shown in Fig. 13.

The repeatability of the pitching angle was 0.3 arc-second ( $1.2 \mu\text{rad}$ ), as shown in Fig. 14, and the repeatability of the linear stage pitching angle was 0.3 arc-second ( $1.4 \mu\text{rad}$ ).

A concave mirror (diameter: 50 mm) was subsequently measured with one-line scanning. Since the measurement range of the autocollimator was smaller than the slope changes of the sample, the rotation stage was rotated 22 times. The raw angle data is shown in Fig. 15.

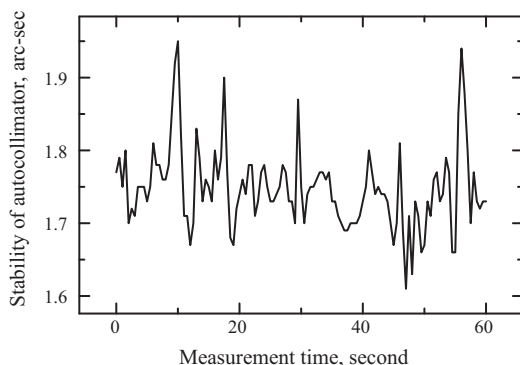


Fig. 12. Drift of autocollimator in 50 s.

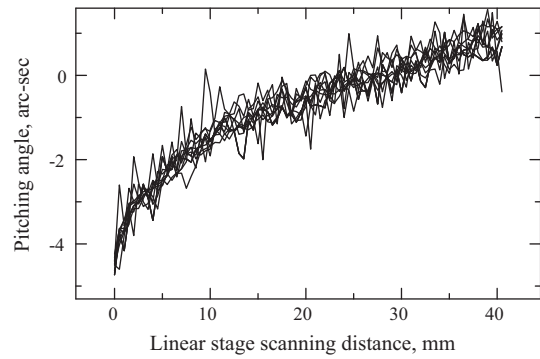


Fig. 13. Pitching error of linear stage measurement result with 10 repeated measurements.

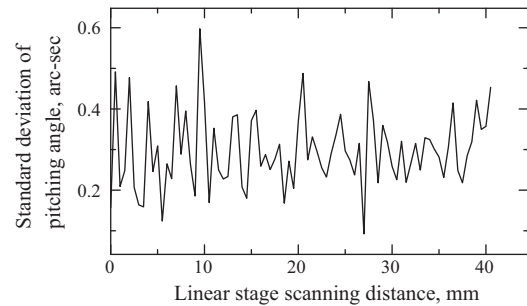


Fig. 14. Standard deviation of pitching angle data of linear stage with 10 measurements.

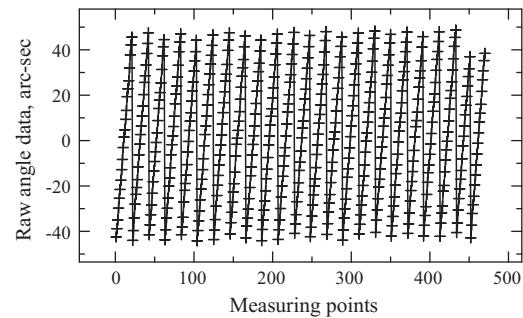


Fig. 15. Raw angle data for measuring a concave mirror with diameter of 50 mm.

By using the data processing method introduced in Section 2, the profile of the sample surface was calculated as shown in Fig. 16.

By using the stability data of the autocollimator, the repeatability of the pitching angle of the linear stage, and the positional repeatability of the linear stage, as listed in Table 3, the random error of the measurement can be predicted.

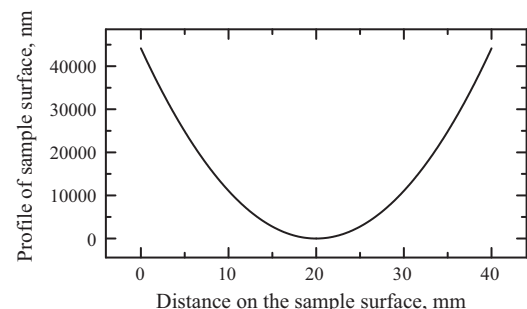


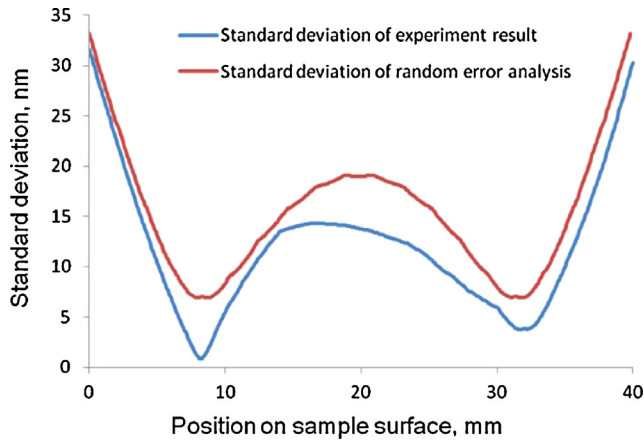
Fig. 16. Profile of the sample surface.

**Table 3**  
Parameters used in the prediction of random error distribution.

	Parameters				
	$L$ (mm)	$R$ (mm)	$h$ (mm)	$A_{max}$ ( $\mu$ rad)	$D$ (mm)
Value	40	5000	0.1	400	100

	Parameters		
	$E_{act}$ ( $\mu$ rad)	$E_x$ ( $\mu$ m)	$E_{rep}$ ( $\mu$ rad)
Value	0.3	1	1.2



**Fig. 17.** Comparison between the simulated random error distribution and deviation from experiment results.

The simulation results were then compared with the experiment results, as shown in Fig. 17. The red line shows standard deviation of random error distribution when the method introduced in Section 3 was used for the calculation, and the blue line shows standard deviation with 10 experiment results.

As shown in Fig. 17, the standard deviation of the experiment results coincides with the simulated error distribution. This implies that the random error analysis has high reliability.

## 5. Conclusion

In this paper, we have proposed a new scanning deflectometry method that includes a rotation stage for the measurement of large aspheric optical surfaces. To predict the measurement repeatability of the proposed method, random error analysis was performed using the error propagation method and Monte Carlo method.

An experiment setup was constructed and a concave mirror with large slope changes was measured successfully. Repeated measurement results showed that the repeatability had very good agreement with the random error analysis results. The random error analysis will be useful in facilities for measuring large aspheric surfaces with high accuracies.

## References

- [1] Martin HM, Angel JRP, Burge JH, Miller SM, Sasian JM, Strittmatter PA. Optics for the 20/20 telescope. *Proceedings of SPIE* 2003;4840:194–205.
- [2] Garbusi E, Osten W. Analytical study of disturbing diffraction orders in in-line computer generated holograms for aspheric testing. *Optics Communications* 2010;283:2651–6.
- [3] Kang G, Xie J, Su P, Tan Q, Jin G. Null test of aspheric surface based on digital phase-shift interferometer. *Optik – International Journal for Light and Electron Optics* 2010;121:1586–90.
- [4] Geckeler RD, Just A, Krause M, Yashchuk VV. Autocollimators for deflectometry: current status and future progress. *Nuclear Instruments and Methods in Physics Research Section A: Accelerators, Spectrometers Detectors and Associated Equipment* 2010;616:140–6.
- [5] Szwedowicz K. 3D deflectometry platform: fast optical scanning technique for inspection of 110 mm silicon wafers. *Stan Ackermans Instituut*; 2003.
- [6] Xiao M, Jujo S, Takahashi S, Takamasu K. Nanometer profile measurement of large aspheric optical surface by scanning deflectometry with rotatable devices: uncertainty propagation analysis and experiments. *Precision Engineering* 2012;36:91–6.
- [7] Taylor JR. *An Introduction to Error Analysis*. The United States of America: University Science Books; 1982.